energy&fuels

Article

pubs.acs.org/EF

Numerical Study of Hydrogen Inhibition of Char Gasification Using Detailed Hetero- and Homogeneous Chemical Kinetics

Joanna Lazar,[†,‡] Nils Erland L. Haugen,[*,‡,§] Jonas Kruger,[‡] and Andrzej Szlek[†]

[†]Silesian University of Technology, Konarskiego 22, 44-100 Gliwice, Poland

[‡]Norwegian University of Science and Technology, 7491 Trondheim, Norway

[§]SINTEF Energy Research, 7465 Trondheim, Norway

ABSTRACT: It has been known for a long time that hydrogen in the gas phase tends to inhibit gasification of char at low and intermediate temperatures. At higher temperatures, however, there are indications that hydrogen may speed up gasification. The mechanisms behind these effects are currently not understood. In this work, a newly developed detailed chemical kinetics model for char has been used to study the mechanisms behind the hydrogen inhibition and speed up of char gasification. For conditions assumed in this work, the hydrogen inhibition is found for $T < 2000$ K, while for $T > 2000$ K, hydrogen in the gas phase speeds up the char conversion. By studying the species reaction rates together with the individual rate of every heterogeneous reaction, the reasons for hydrogen influence on char gasification are attempted to be explained for a wide range of different temperatures in this paper. The focus is not on investigating a real gasifier but rather to understand the fundamental mechanism behind hydrogen inhibition of char.

INTRODUCTION

For many applications, it is not feasible or just not economical to use solid fuels directly. It is therefore often useful to convert the solid fuel to either a gaseous or liquid fuel before it is used. Solid fuels, such as, e.g., coal, biomass, or pet coke, can be converted to a synthesis gas (syngas) through reactions with oxygen, steam, or carbon dioxide in a gasifier. The syngas can then be used for, e.g., electricity production in an integrated gasification combined cycle (IGCC), production of liquid fuels for the transportation sector, or production of hydrogen for fuel cells or use in the chemical industry.

The newly developed detailed heterogeneous chemical kinetics model of Tilghman and Mitchell,[1] with 18 reversible reactions for char reactions with oxygen, steam, and carbon dioxide, has been used in the current work. Hecht et al.[2] have shown that, in oxygen-fired systems, it is important to include the effects of CO_2 gasification. The chemical mechanism is used to study the mechanism behind the hydrogen inhibition of char gasification at low and intermediate temperatures. The effect of a speed up of the gasification process at higher temperatures has also been studied. To check the impact of hydrogen on the char gasification, without changing the thermodynamics of the fluid, the heterogeneous reactions that have gaseous molecular hydrogen as a reactant are turned on and off; i.e., the impact of a given reaction where hydrogen is a reactant is investigated by comparing the results obtained when that specific reaction is turned off with the results obtained when all reactions are turned on. In this way, the impact of hydrogen on the gasification process can be studied in great detail. The respective reactions are turned off by setting their pre-exponential factors to zero.

For low temperatures or small char particles, the conversion rate is kinetically controlled and the pore surface of the entire particle volume is reacting. This, which is known as zone I conversion, yields a constant particle radius, where the particle mass is reduced by a decrease in density. For very high temperatures or large particles, the reactants are consumed at the external surface of the particles. This decreases the particle radius while keeping the density constant and is known as zone III conversion. Zone II conversion, on the other hand, is observed for intermediate temperatures and particle sizes. For this regime, both particle radius and density are decreased and the relative fraction of decrease is described by Haugen et al.[3]

The effect of hydrogen inhibition on surface reactions was also recently studied by Pineda and Chen.[4] Here, the authors use a heterogeneous reaction mechanism consisting of eight reaction steps in a perfectly stirred reactor to find that the inhibition of hydrogen is due to the adsorbed molecular hydrogen filling up a significant fraction of all of the free sites on the carbon surface.

Hydrogen inhibition has previously been studied under many different gasifying conditions. One of the earlier discussions on the reaction mechanism behind hydrogen inhibition is found by Laurendeau.[5] In previous experimental work, inhibition has been observed at low (1 atm) and moderate (10 atm) steam pressures and moderate temperatures (950−1250 K)[6−10] as well as at high pressures (40−50 atm).[11,12] For gasification of a natural graphite at temperatures between 960 and 1120 °C and low pressures, Biederman et al.[8] found that hydrogen inhibition was caused by dissociative chemisorption of hydrogen on active carbon sites. For graphite−CO_2 reactions, they found that the inhibition was due to hydrogen chemisorbing on impurity catalyst sites. Barrio et al. studied the steam gasification of wood at atmospheric pressure and in the temperature range from 750

Special Issue: International Symposium on Combustion Processes

Received: March 2, 2016
Revised: April 6, 2016

DOI: 10.1021/acs.energyfuels.6b00502
Energy Fuels XXXX, XXX, XXX−XXX

Table 1. Intrinsic Heterogeneous Reaction Mechanism[a]

number	reaction	A_k	E_k	σ_k
R1	$2C_f + H_2O \leftrightarrow C(OH) + C(H)$	2.1×10^6	105	0
R2	$C(OH) + C_f \leftrightarrow C(O) + C(H)$	4.1×10^{11}	80	0
R3	$C(H) + C(H) \leftrightarrow H_2 + 2C_f$	1.4×10^{11}	67	0
R4	$C(O) + C_b \rightarrow CO + C_f$	1.0×10^{13}	353	28
R5	$C(OH) + C_b \leftrightarrow HCO + C_f$	1.0×10^{13}	393	28
R6	$C_b + C_f + C(H) + H_2O \leftrightarrow CH_3 + C(O) + C_f$	1.0×10^{13}	300	0
R7	$C_b + C_f + C(H) + H_2 \leftrightarrow CH_3 + 2C_f$	1.0×10^{13}	300	0
R8	$C_f + C(H) + CO \rightarrow HCO + 2C_f$	1.0×10^{13}	300	0
R9	$C(H) + C(H) \rightarrow CH_2 + C_f$	3.0×10^{11}	426	0
R10	$CO_2 + C_f \leftrightarrow C(O) + CO$	3.7×10^3	161	0
R11	$C_b + CO_2 + C(O) \rightarrow 2CO + C_f$	1.26×10^8	276	0
R12	$C(CO) \leftrightarrow CO + C_f$	1.0×10^{13}	455	53
R13	$CO + C(CO) \rightarrow CO_2 + 2C_f$	9.8×10^6	270	0
R14	$2C_f + O_2 \rightarrow C(O) + CO$	5.0×10^{10}	150	0
R15	$2C_f + O_2 \rightarrow C_2(O_2)$	4.0×10^7	93	0
R16	$C_f + C_b + C(O) + O_2 \rightarrow CO_2 + C(O) + C_f$	1.5×10^7	78	0
R17	$C_f + C_b + C(O) + O_2 \rightarrow CO + 2C(O)$	2.1×10^7	103	0
R18	$C_b + C_2(O_2) \rightarrow CO_2 + 2C_f$	1.0×10^{13}	304	33

[a]The units of both the activation energy E_k and the distribution width σ_k are kJ/mol, while the units of A_k are such that the units of $R_{reac,c}$ in eq 9 are mol m^{-2} s^{-1}.

to 950 °C.[10] In their work, it is concluded that the hydrogen inhibition effect can be described on the basis of Langmuir–Hinshelwood kinetics. The aim of the work of Tay et al.[13] was to investigate the role of hydrogen during the gasification of a Victorian brown coal at 800 °C in a fluidized-bed/fixed-bed reactor. Here, it was found that the inhibiting effects of hydrogen were not limited to its chemisorption on the char surface. The presence of hydrogen also changed the aromatic structure of char during gasification, which is most likely due to the ability of hydrogen radicals to penetrate into the char matrix. In the work of Fushimi et al.[14] on steam gasification of woody biomass char, it was observed that hydrogen inhibition was due to reverse oxygen exchange reactions in the first period and dissociative hydrogen adsorption on the char particle in the second period.

In the current work, the focus is on gasification of char from Wyodak coal, which is a sub-bituminous coal from Wyoming, U.S.A. It is expected, however, that the results should also be similar for other fuels, such as, e.g., other coal qualities or biomass.

MODEL DESCRIPTION

In this section, the essentials of the numerical model used to simulate the char gasification are described. The implementation of the numerical model has been verified by Haugen et al.[3] against the particle-resolved simulation tool (DNS) of the Stanford group. For more information on the model, the reader is referred to the study by Haugen et al.[15]

In the following, particles are assumed to be spherical and uniform in composition and morphology, while the ash is uniformly distributed throughout the particle volume. In addition, ash in the char cannot react or be evaporated, and there is no exchange of mineral matter between the particle and the gas phase.

The calculations are made on a single particle in the particle cloud. It is assumed that all other particles behave in the same way as the considered particle. The carbon in the particle will react with the hot reactive gases (O_2, H_2O, and CO_2), causing the mass, apparent density, and size of the particle to change with time. The heterogeneous chemical kinetics were developed by Tilghman and Mitchell[1] based on the work of Haynes[16] and are presented in Table 1, while the homogeneous chemical kinetic mechanism used is GRI-Mech 3.0.[17] The ultimate and proximate analyses of the coal are presented in Tables 2 and 3. In the heterogeneous reaction scheme, the adsorbed species C(H), C(O), C(CO), and C(OH) represent a hydrogen atom, oxygen atom, carbon monoxide, and OH group adsorbed on a carbon site, respectively, while $C_2(O_2)$ represent two adjacent carbon sites that have adsorbed one oxygen atom each. The bulk carbon site, C_b, is a carbon atom bonded to four other carbon atoms. As a result of chemical reactions, the bulk carbon site can become a free carbon site. The free carbon site, C_f, is a carbon atom that is available for adsorption of gas-phase species. As a result of the particle–gas reactions, the oxygen, carbon, and hydrogen compounds desorb from the carbonaceous matrix and leave the particle surface. As a result of this process, an underlying carbon atom becomes a free carbon site.

Table 2. Proximate Analysis of Wyodak Coal

property	amount (wt %)
fixed carbon	35.06
volatile matter	33.06
moisture	26.30
ash	5.58

Table 3. Ultimate Analysis of Wyodak Coal

property	amount (wt %)
carbon	69.8
hydrogen	5.65
oxygen (by difference)	15.6
nitrogen	0.94
total sulfur	0.43
ash	7.57

Arrhenius parameters shown in Table 1 were obtained for Wyodak coal[1] based on thermogravimetric analysis (TGA). The obtained activation energies where found to be within expected ranges when compared to values for chars and activated carbon from the literature. In the experiments, the char conversion was limited only by the chemical reaction rates; i.e., the experiments were kinetically controlled. The pressure was held at 1 atm, and the testing temperatures were selected according to the reacting gases: 700–900 °C for environments containing H_2O, 800–1000 °C for

DOI: 10.1021/acs.energyfuels.6b00502
Energy Fuels XXXX, XXX, XXX–XXX

environments containing CO_2, and 400−550 °C for environments containing O_2. The char specific surface area was measured with the Brunauer−Emmett−Teller (BET) method. Because the heterogeneous reaction mechanism is intrinsic, the surface area is required to calculate the total reaction rate of the char particle.

In this paper, the focus is on the two reactions that have molecular hydrogen as a reactant. This corresponds to reaction R3 backward (R3b) and reaction R7 forward (R7f). Hydrogen inhibition of char gasification is studied by investigating the effect of deactivating these two reactions.

The exchange of matter between the particles and the ambient gas is caused by reactions between the gas and the solid phase. The species production rate can be symbolized by $\omega_{pg,i}$ for the particle−gas reactions and $\omega_{gg,i}$ for the gas−gas reactions. These two terms determine the change of the mass fraction of species i in the gas phase.

Governing Gas-Phase Equations. In the following, a brief overview of the most important equations will be presented. For a full description of all relevant equations, the reader is referred to the study by Haugen et al.[15]

The gas phase is defined by three governing equations describing the evolution of mass, species, and temperature in the gas phase. The first equation describes the evolution of the mass of the gas phase m_g

$$\frac{dm_g}{dt} = \frac{m_g}{\rho_g}\sum_{i=1}^{N_{s,gas}} \omega_{pg,i} M_i \tag{1}$$

where ρ_g is the mass density of the gas phase, M_i is the molar mass of species i, and $\omega_{pg,i}$ is the molar production rate of species i as a reactions between the solid and the gas phase (heterogeneous reactions). The second equation describes the mass fraction Y_i of species i in the gas phase

$$\rho_g \frac{dY_i}{dt} + Y_i \sum_{k=1}^{N_{s,gas}} \omega_{pg,k} M_k = (\omega_{gg,i} + \omega_{pg,i}) M_i \tag{2}$$

where $\omega_{gg,i}$ is the molar production rate of species i as a result of gas-phase (homogeneous) reactions. The third equation is the energy equation, which is represented here by the temperature

$$\rho_g c_{p,g} \frac{dT_g}{dt} + \sum_{i=1}^{N_{s,gas}} h_i(\omega_{gg,i} + \omega_{pg,i}) M_i = n_p(Q_h + Q_c) \tag{3}$$

where $c_{p,g}$ is the heat capacity of the gas mixture at a constant pressure, T_g is the temperature of the gas, h_i is the enthalpy of species i, Q_h is the energy transfer from the solid phase to the gas phase as a result of heterogeneous reactions, and Q_c is the heat transfer from the particle to the gas mixture as a result of convection and conduction.

Governing Solid-Phase Equations. In this subsection, the governing equations describing mass transport and chemical reactions in the solid phase (the char) are presented.

Particle Mass. The evolution of the carbonaceous part of the char particle mass m_c is described by

$$\frac{dm_c}{dt} = -S_t M_c R_{reac,c} \tag{4}$$

where M_c is the molar mass of carbon and $R_{reac,c}$ is the molar reaction rate of carbon. Because the heterogeneous reaction mechanism is intrinsic, the total surface area of the carbonaceous part of the particle, S_t, is required. This is in contrast to apparent reaction mechanisms, where the effect of the surface area is implicitly included in the reaction kinetics.

Particle Temperature. The temperature evolution of the char particle is given by

$$\frac{dT_p}{dt} = \frac{1}{m_p c_{p,p}}(Q_{reac} - Q_c + Q_{rad}) \tag{5}$$

where T_p is the particle temperature, $c_{p,p}$ is the specific heat capacity of the particle, Q_{reac} is the heating as a result of the heterogeneous reaction, Q_c is the heat transfer from the char particle to the gas phase via convection and conduction, and Q_{rad} is the heating as a result of radiation.[18]

Adsorbed Species. The number of moles of adsorbed species j is given by

$$N_j = C_{s,j} S_t \tag{6}$$

where $C_{s,j}$ is the concentration of adsorbed species j on the surface of the char particle. The rate of change in the site fraction of adsorbed species j is given by

$$\frac{d\Theta_j}{dt} = \frac{R_{spec,j}}{\xi_n} + A R_{reac,c} \Theta_j \tag{7}$$

where $\Theta_j = C_{s,j}/\xi_n$ is the adsorbed species site fraction and ξ_n is the total surface concentration of carbon sites (both free and occupied). The molar rate of adsorbed species production is given by $R_{spec,j}$, while A is an active surface area.[15]

Species Concentrations at the Particle Surface. The relationship between the flux of gas-phase species i through the boundary layer to the external particle surface and the net production of species i via particle−gas reactions, in steady state, is given by

$$\dot{n}_i - X_{i,s}\dot{n}_{total} = -k_{im}(X_{i,\infty} - X_{i,s}) \tag{8}$$

where $X_{i,\infty}$ is the mole fraction of species i in the ambient gas phase and $X_{i,s}$ is the mole fraction of species i at the particle surface. The species mass transfer coefficient is represented by k_{im}. The molar flux of species i, $\dot{n}_i$, is defined as positive in the direction away from the particle surface, such that the total molar flux away from the particle is given by $\dot{n}_{total} = \sum \dot{n}_i$. A Newton method is used to solve eq 8.

Internal Particle Burning and the Effectiveness Factor. The molar rate of reaction k is given by

$$R_{reac,k} = k_k \prod_{i=1}^{N_{s,gas}+N_{s,ads}} C_i^{\nu_{i,k}} \tag{9}$$

where k_k is the rate coefficient of reaction k. The concentration of species i is represented by C_i, while $\nu_{i,k}$ is the stoichiometric coefficient. This equation is valid when the concentration of reactants of reaction k inside the particle is uniform. In a situation where the mass transport rates are slower than the chemical reaction rates, the gas does not penetrate the particle completely. As a result, the concentration of reactants inside the particle is not uniform and the rate of reaction k is lower than what is found from eq 9. The reduced rate of reaction k can be written as

$$R_{reac,k} = \eta_k k_k \prod_{i=1}^{N_{s,gas}+N_{s,ads}} C_i^{\nu_{i,k}} \tag{10}$$

where

$$\eta_k = \frac{3}{\phi}\left[\frac{1}{\tanh(\phi)} - \frac{1}{\phi}\right] \tag{11}$$

is the effectiveness factor of reaction k and ϕ is the Thiele modulus.[19]

The evolution of the particle radius versus density is also handled on the basis of the effectiveness factor, as described by Haugen et al.[3]

RESULTS

To investigate the effect of molecular hydrogen in the gas phase on the heterogeneous reactions, the heterogeneous reactions containing molecular hydrogen as a reactant are either activated or deactivated. The reactions are deactivated by setting their reaction rates to zero. All other conditions are kept unchanged. The first relevant reaction is the reverse part of reaction R3, which in the following is referred to as R3b:

$$H_2 + 2C_f \rightarrow C(H) + C(H) \tag{12}$$

DOI: 10.1021/acs.energyfuels.6b00502
Energy Fuels XXXX, XXX, XXX−XXX

where two free carbon sites on the particle surface and a hydrogen molecule react to become two adjacent carbon sites that each have an adsorbed hydrogen atom. The other relevant reaction is the forward part of reaction R7 (R7f)

$$C_b + C_f + C(H) + H_2 \rightarrow CH_3 + 2C_f \quad (13)$$

where the free carbon site adsorbs the hydrogen molecule from the gas phase. During the process of reaction, the hydrogen molecule moves, binds to the hydrogen atom adsorbed on the carbon site C(H), and desorbs and leaves the particle as CH_3. An underlying bulk carbon becomes a free carbon site.

By turning on and off reactions R3b and R7f, four different test cases can be defined, as presented in Table 4. The purpose of this paper is to investigate the impact of H_2 in the gas phase on the time that is needed to reach full conversion of the char particle and to understand the reasons of this impact. It is assumed that full conversion of a particle is reached when 99% of the solid carbon has been converted.

Table 4. Studied Cases A, B, C, and D[a]

case	R3b	R7f
case A	on	on
case B	off	on
case C	on	off
case D	off	off

[a]Reaction R3b, $H_2 + 2C_f \rightarrow C(H) + C(H)$, and reaction R7f, $C_b + C_f + C(H) + H_2 \rightarrow CH_3 + 2C_f$, are simulated to be active or not active.

In the following, the impact of hydrogen in the gas phase on char gasification at low, intermediate, and high temperatures is studied. It is assumed that the temperatures of the fluid and the particles inside the reactor during the conversion process is constant. Small char particles, with Stokes numbers less than unity, are used. Furthermore, the reactor is assumed to be perfectly stirred within a small sub-volume following the particles, such that both species and particles are homogeneously distributed within this sub-volume. This means that the char particles stay within the fluid element into which they where injected throughout the course of conversion. As such, the process can be thought of as a batch process for each particle, even though the reactor itself is continuous. The exception from the homogeneity of the simulation domain is the thin boundary layer around each char particle, where gradients in gas-phase species exist as described by eq 8. It is clear that the assumption of a constant gas temperature is not valid in a real application; this assumption is nevertheless made to more clearly see the effect of the temperature on the reactions and, correspondingly, also on the amount of hydrogen inhibition.

It should also be noted that in real gasification of coal, the properties of the char will depend upon the conditions under which the char was formed. This effect is not accounted for here, and all char samples have been formed under the same conditions.

Conversion of the char particle exposed to the conditions shown in Table 5 and reacting according to the set of reactions presented in Table 1 describe the base case simulation (case A). See Table 4 for a description of the other cases (B, C, and D).

The time to reach full conversion as a function of the temperature is shown in Figure 1. The time to reach full conversion is symbolized by τ. At high temperatures ($T > 1900$ K), it takes less than 1 s to reach full conversion. It can also be seen that, in the temperature range of 1150−2000 K, the full conversion is reached faster for cases B and D than for cases A and C. At low temperatures ($T < 1400$ K), it can be observed that τ is longer for case C than for case A. In the temperature range of 2000−2650 K, it takes longer to reach full conversion for cases B and D than for cases A and C. On the basis of this, it is clear that the impact of hydrogen on the char gasification strongly depends upon the gasification temperature.

Table 5. Properties for the Simulation at a Constant Temperature Inside the Reactor

property	value	unit
carbon/gas mole ratio	0.5	
reactor wall temperature	700	K
pressure	2.4×10^6	Pa
initial particle radius	5.0×10^{-5}	m
initial particle density	1300	kg/m^3
initial mole fraction of H_2O	0.50	
initial mole fraction of O_2	0.45	
initial mole fraction of N_2	0.05	

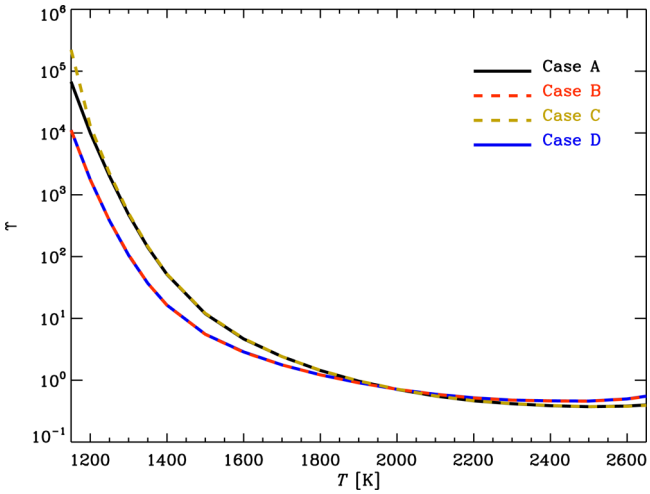

Figure 1. Time to reach full conversion of the char as a function of the temperature.

Let us now compare the time that it takes for the char to reach full conversion in each case, where one of the hydrogen reactions (cases B and C) or both of them (case D) are deactivated, with the time it takes to reach full conversion in the base case (case A), in different temperatures. This relationship can be expressed by the ratio of the time to reach full conversion in cases B, C, and D, respectively, to the time to reach full conversion in case A. These ratios are symbolized by α and can be written as

$$\alpha_B = \frac{\tau_B}{\tau_A}, \quad \alpha_C = \frac{\tau_C}{\tau_A}, \quad \text{and} \quad \alpha_D = \frac{\tau_D}{\tau_A} \quad (14)$$

when τ_A, τ_B, τ_C, and τ_D represent the time to reach full conversion in cases A, B, C, and D, respectively.

In Figure 2, the relative time to reach full conversion of the char as a function of the temperature for cases with (black line) and without (colored lines) hydrogen reactions is shown. It can be seen that α_B and α_D increase with an increasing temperature, reach unity at about 2000 K, and continue to increase. It is also seen that α_C decreases with an increasing temperature, reaches unity at about 1400 K, and remains equal to unity at higher temperatures.

DOI: 10.1021/acs.energyfuels.6b00502
Energy Fuels XXXX, XXX, XXX−XXX

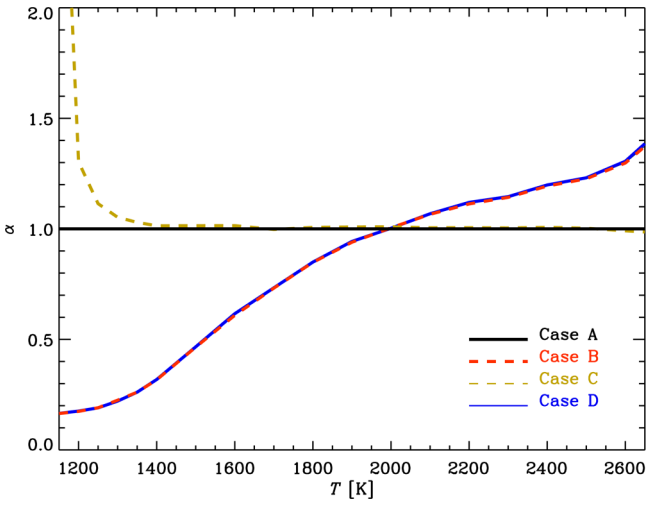

Figure 2. Relative time to reach full conversion of the char as a function of the temperature.

By comparison of cases A and B, it is seen that hydrogen in the gas phase inhibits char gasification at low and intermediate temperatures (T < 2000 K), while hydrogen speeds up the gasification process at high temperatures (T > 2000 K). By comparison of cases B and D, it also seems clear that reaction R7f does not have a significant impact on the results and, hence, that the hydrogen inhibition is primarily due to reaction R3b.

To study the exact mechanism behind the impact of hydrogen on char gasification, the gasification process has been studied in detail for three selected temperatures. The lowest temperature (1150 K) corresponds to the lowest temperature for which full conversion could be reached; the intermediate temperature (2000 K) corresponds to the temperature where the time to reach full conversion both with and without the hydrogen reactions turned on are equal; and the higher temperature (2650 K) corresponds to the highest temperature where a numerical result could be obtained.

The mechanism employed in this work is designed to study the process of gasification at low and intermediate temperatures. However, in this section, the mechanism has been used to simulate char gasification in a much wider temperature range. It will later become evident when studying the species production rates that the heterogeneous mechanism is "unstable" at very high temperatures of ~2600 K. This clearly means that the mechanism cannot be fully trusted at these high temperatures. These problems do not, however, seem to have any substantial impact on the overall results. By "unstable", it is meant that the simulation code is not able to identify one single solution but rather jumps between two neighboring possible solutions.

Gasification at 1150 K. At a temperature of 1150 K, turning off reaction R3b slows the overall production of C(H), which is seen by comparing cases A and B in Figure 3. Because C(H) is a reactant in reaction R1b, $2C_f + H_2O \leftrightarrow C(OH) + C(H)$, and reaction R2b, $C(OH) + C_f \leftrightarrow C(O) + C(H)$, the molar rate of both reactions R1 and R2 is higher when reaction R3b is deactivated. The net result of this is that more C(O) is produced, which leads to higher molar rates of reaction R4, $C(O) + C_b \rightarrow CO + C_f$, reaction R10b, $CO_2 + C_f \leftrightarrow C(O) + CO$, and reaction R11, $C_b + CO_2 + C(O) \rightarrow 2CO + C_f$. In

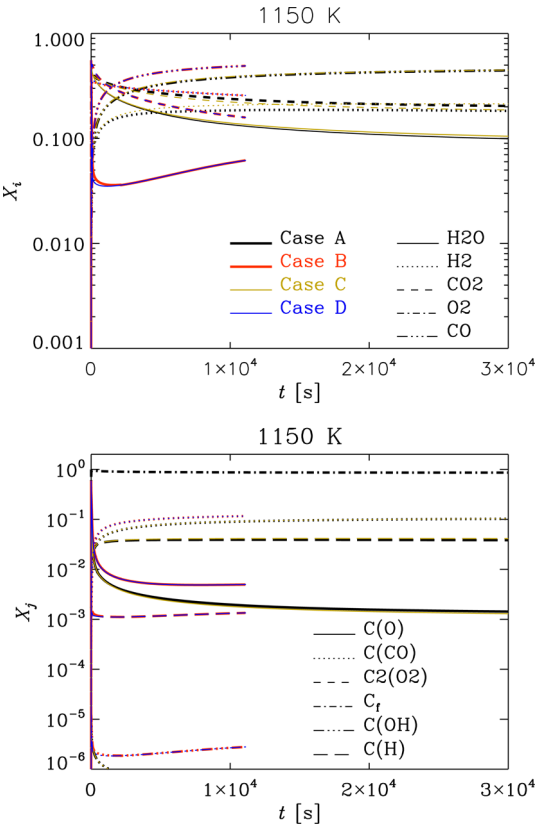

Figure 3. Gas-phase species fraction X_i (top panel) and surface fraction X_j of adsorbed species (bottom panel) as a function of time at a temperature of 1150 K.

reactions R4 and R11, a carbon atom is removed from the solid surface, and as such, these reactions have a positive impact on the conversion rate of the char. Because reaction R10 is neutral with respect to its impact on the conversion, the increased conversion rate of the char when reaction R3b is turned off is due to the higher amount of adsorbed oxygen on the surface when there is less adsorbed hydrogen present.

When reaction R7f is deactivated, we see from eq 2 that the time to reach full conversion increases for very low temperatures. The reason for this is 2-fold: first, the deactivation of reaction R7f yields a higher concentration of adsorbed hydrogen, which, as described in the previous paragraph, has a negative effect on the rate of conversion. It can, however, be seen from Figure 3 that the levels of adsorbed hydrogen and oxygen are rather similar for cases A and C, such that this effect is not expected to be significant. Second, because reaction R7f removes one carbon from the solid surface, the deactivation of this reaction will also reduce the rate of conversion directly. This is probably the main reason for the longer times to reach full conversion when reaction R7f is turned off for temperatures less than 1400 K.

Gasification at Higher Temperatures. In this section, the gasification characteristics at temperatures of 2000 and 2650 K are presented. It should be noted that, at these high temperatures, the assumption that the ash cannot evaporate is no longer valid.

From Figure 2, it can be seen that the deactivation of reaction R3b, at a temperature of 2000 K, does not influence the net rate of conversion. The main reason that the deactivation of reaction R3b does not have an effect at this

DOI: 10.1021/acs.energyfuels.6b00502
Energy Fuels XXXX, XXX, XXX−XXX

temperature, even though the effect was substantial at 1150 K, is that the deactivation of reaction R3b no longer has an effect on the amount of adsorbed oxygen on the particle surface. This can be seen by comparing cases A and B in the lower panel of Figure 4.

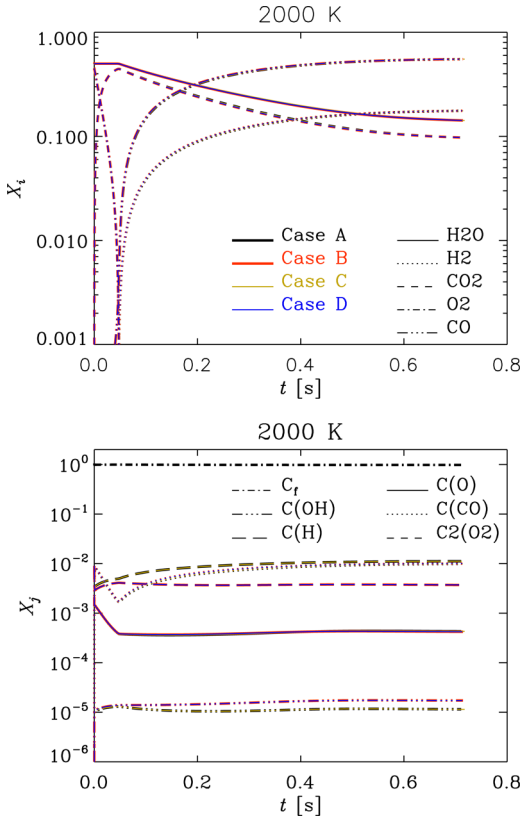

Figure 4. Gas-phase species fraction X_i (top panel) and surface fraction X_j of adsorbed species (bottom panel) as a function of time at a temperature of 2000 K.

As a result of the lower concentration of C(H), reaction R8 slows. This does not have an effect on the char conversion rate, because reaction R8 does not change the number of carbon atoms on the surface, but it does affect the net production rate of CO and HCO. This can be seen by comparing cases A and B in Figure 5. On the basis of the above, it may at first glance seem surprising that the molar concentrations of CO and HCO in the gas phase are still unchanged. This is however due to the fact that these species are converted through the homogeneous reactions to obtain chemical equilibrium in the gas phase. At these high temperatures, gas-phase chemical equilibrium is obtained at a time scale significantly shorter than the time scale for char conversion.

In Figure 4, the gas-phase species concentration X_i and surface species concentration X_j as a function of time at a temperature of 2000 K is shown. The gas phase reaches chemical equilibrium because the difference between the fractions of each species cannot be seen. The important difference is between cases A and B for the concentration of hydrogen adsorbed on the particle surface, which is higher in case A, because C(H) is not produced as a result of reaction R3b.

By studying Figure 6, it can be seen that several of the adsorbed species fractions make abrupt and seemingly

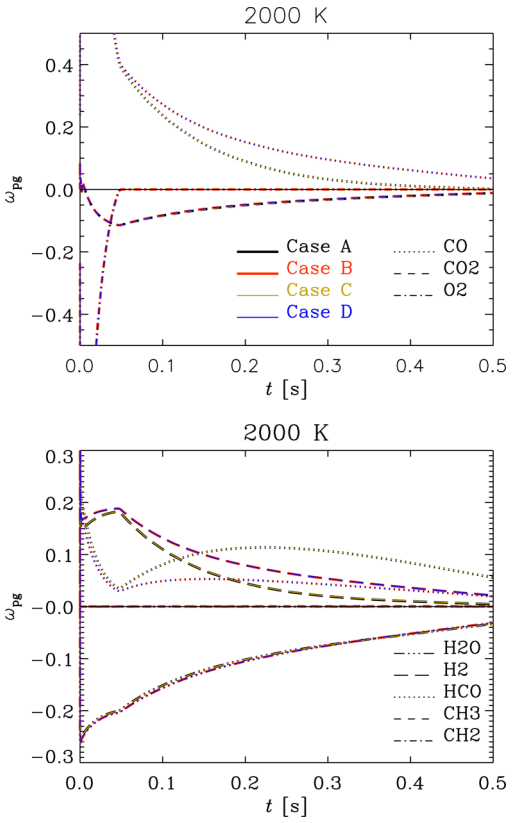

Figure 5. Species production rate ω_{pg} as a result of the gas−particle reactions as a function of time at a temperature of 2000 K.

unphysical jumps. Because smooth numerical results are no longer obtained, this indicate that a temperature of 2650 K is outside the temperature range for which the heterogeneous mechanism can be used. The reason for these jumps in adsorbed species fractions is probably that there exist two different solutions that both satisfy the governing equations at these rather extreme conditions. The numerical solver then ends up jumping between these two solutions, which yields the observed jumps in adsorbed species fractions.

Gasification at Very Low Temperatures. At low temperatures, global chemical equilibrium dictates that full conversion of the char will not be obtained. For the conditions presented in Table 5, it is found that the char is fully converted for $T > 1150$ K. Below this temperature, only a fraction of the char will be converted as $t \rightarrow \infty$.

The fraction of the char that becomes converted is visualized by the solid lines in Figure 7. Here, it is seen that the amount of conversion decreases with the temperature for all cases but that the cases when reaction R3b is turned off always yield more conversion. The explanation for this is the same as before, namely, that less adsorbed hydrogen on the surface yields more adsorbed oxygen and, hence, more char conversion through reaction R4. The conversions shown here are obtained as time goes toward infinity, i.e., at chemical equilibrium. Hence, these results can be compared to results from chemical equilibrium solvers. Here, GASEQ[20] and Cantera[21] have been used to simulate the equilibrium condition. These results are visualized by the deep red dashed−dotted line and the black dashed line in Figure 7. From this, it is seen that the results for the two equilibrium solvers are almost identical, as expected, and that the trends obtained from the equilibrium solvers are similar to

DOI: 10.1021/acs.energyfuels.6b00502
Energy Fuels XXXX, XXX, XXX−XXX

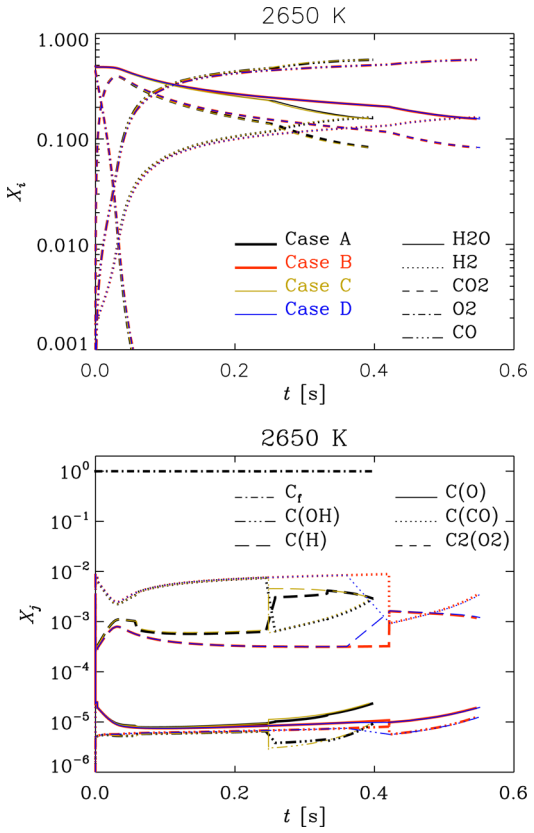

Figure 6. Gas-phase species fraction X_i (top panel) and surface fraction X_j of adsorbed species (bottom panel) as a function of time at a temperature of 2650 K.

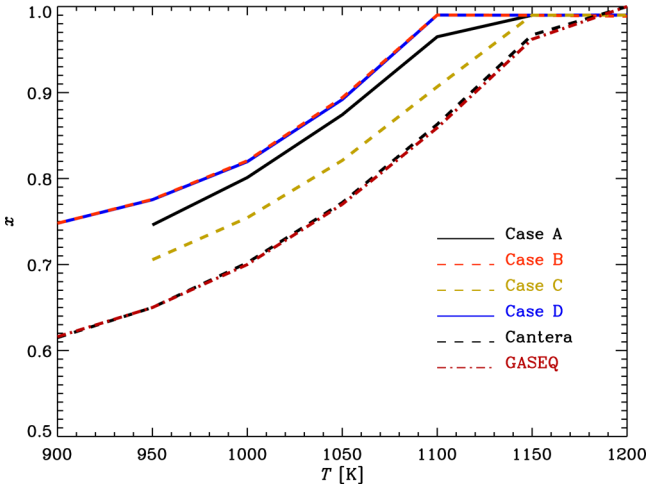

Figure 7. Conversion as a function of the temperature for different cases and two different equilibrium solvers.

what is found for cases A–D. The equilibrium solvers do, however, always yield a slightly lower conversion. Because one or more of the reactions are turned off in cases B–D, these cases are not expected to yield results similar to the equilibrium solvers. This is not true for case A, however. The reason for the discrepancy between the equilibrium solvers and case A is the fact that the equilibrium solvers do not take the adsorbed species into account. This means that the enthalpies and entropies of the char in the equilibrium solvers are not the same as in our main solver; hence, the Gibbs free energy and, correspondingly, also the equilibrium condition are different.

SUMMARY

In this work, the newly developed detailed chemical kinetics model of Tilghman and Mitchell[1] has been used to study the mechanisms behind hydrogen inhibition and speed up of char gasification. For the conditions studied here, it is clearly seen that hydrogen inhibition is found for $T < 2000$ K, while for $T > 2000$ K, hydrogen in the gas phase speeds up the char conversion. By studying the species reaction rates together with the individual rate of every single reaction, it is shown that hydrogen inhibition at low and intermediate temperatures is due to atomic hydrogen adsorbed on the char surface interacting with atomic oxygen on the surface to form an adsorbed OH molecule. The adsorbed OH molecule combines with another adsorbed hydrogen atom to form gaseous water. The outcome of this is that adsorbed atomic oxygen, which would normally desorb as gaseous CO while removing a carbon atom from the surface, only takes part in the production of steam, which does not yield any char conversion, and hence, the time to reach full conversion is increased as a result of the presence of hydrogen. This conclusion differs from the findings of Pineda and Chen,[4] who found that hydrogen inhibition is mainly due to the blocking of active sites by adsorbed hydrogen. This discrepancy may be explained by the fact that adsorbed OH was not a part of of their mechanism.

It has also been shown that, at higher temperatures, the presence of hydrogen results in a speed up of the char conversion. This is primarily due to reaction 6f, where adsorbed hydrogen reacts with steam to produce oxygen adsorbed on the surface. As a result of the higher concentration of C(O), the process of removing carbon from the surface is faster.

AUTHOR INFORMATION

Corresponding Author

*E-mail: nils.e.haugen@sintef.no.

Notes

The authors declare no competing financial interest.

ACKNOWLEDGMENTS

This work forms part of the CAMPS project supported by the Research Council of Norway (215707). The work has additionally been produced with support from the BIGCCS Centre, performed under the Norwegian Research Program Centres for Environment-Friendly Energy Research (FME). The author acknowledges the following partners for their contributions: Aker Solutions, ConocoPhillips, Gassco, Shell, Statoil, TOTAL, GDF SUEZ, and the Research Council of Norway (193816/S60). The research leading to these results has received funding from the Polish–Norwegian Research Programme operated by the National Centre for Research and Development under the Norwegian Financial Mechanism 2009–2014 in the frame of Project Contract Pol-Nor/232738/101/2014. Nils Erland L. Haugen also acknowledges the Research Council of Norway under the FRINATEK Grant 231444. This work has also benefitted from the WoodCFD project, which is funded by: Dovre AS, Norsk Kleber AS, Jøtulgruppen and Morsø AS together with the Research Council of Norway through the ENERGIX program (243752/E20).

DOI: 10.1021/acs.energyfuels.6b00502
Energy Fuels XXXX, XXX, XXX–XXX

REFERENCES

(1) Tilghman, M. B.; Mitchell, R. E. Coal and biomass char reactivities is gasification and combustion environments. *Combust. Flame* **2015**, *162*, 3220−3235.

(2) Hecht, E. S.; Shaddix, C. R.; Molina, A.; Haynes, B. S. Effect of CO_2 gasification reaction on oxy-combustion of pulverized coal char. *Proc. Combust. Inst.* **2011**, *33*, 1699−1706.

(3) Haugen, N. E. L.; Mitchell, R. E.; Tilghman, M. B. The conversion mode of a porous carbon particle during oxidation and gasification. *Combust. Flame* **2014**, *161*, 612.

(4) Pineda, D. I.; Chen, J.-Y. Modeling hydrogen inhibition in gasification surface reactions. *Int. J. Hydrogen Energy* **2015**, *40*, 6059.

(5) Laurendeau, N. M. Heterogeneous kinetics of coal char gasification and combustion. *Prog. Energy Combust. Sci.* **1978**, *4*, 221−270.

(6) Gadsby, J.; Hinshelwood, C. N.; Sykes, K. W. The Kinetics of the Reactions of the Steam-Carbon System. *Proc. R. Soc. London, Ser. A* **1946**, *187*, 129−151.

(7) Johnstone, H. F.; Chen, C. Y.; Scott, D. S. Kinetics of the steam-carbon reaction in porous graphite tubes. *Ind. Eng. Chem.* **1952**, *44* (7), 1564−1569.

(8) Biederman, D. L.; Miles, A. J.; Vastola, F. J.; Walker, P. L., Jr. Carbon-carbon dioxide reaction: kinetics at low pressures and hydrogen inhibition. *Carbon* **1976**, *14*, 351−356.

(9) Hüttinger, K. J.; Merdes, W. F. The carbon-steam reaction at elevated pressure: formations of product gases and hydrogen inhibitions. *Carbon* **1992**, *30* (6), 883−894.

(10) Barrio, M.; Gøbel, B.; Rimes, H.; Henriksen, U.; Hustad, J. E.; Sørensen, L. H. Steam gasification of wood char and the effect of hydrogen inhibition on the chemical kinetics. In *Progress in Thermochemical Biomass Conversion*; Bridgwater, A. V., Ed.; Blackwell Science, Ltd.: Oxford, U.K., 2001; Chapter 2, pp 32−46, DOI: 10.1002/9780470694954.ch2.

(11) Mühlen, H.-J.; van Heek, K. H.; Jüntgen, H. Kinetic studies of steam gasification of char in the presence of H_2, CO_2 and CO. *Fuel* **1985**, *64* (7), 944−949.

(12) Moilanen, A.; Mühlen, H.-J. Characterization of gasification reactivity of peat char in pressurized conditions effect of product gas inhibition and inorganic material. *Fuel* **1996**, *75* (11), 1279−1285.

(13) Tay, H.-L.; Kajitani, S.; Zhang, S.; Li, C.-Z. Inhibiting and other effects of hydrogen during gasification: Further insights from FT-Raman spectroscopyl. *Fuel* **2014**, *116*, 1−6.

(14) Fushimi, C.; Wada, T.; Tsutsumi, A. Inhibition of steam gasification of biomass char by hydrogen and tar. *Biomass Bioenergy* **2011**, *35* (1), 179−185.

(15) Haugen, N. E. L.; Mitchell, R. E.; Tilghman, M. B. A comprehensive model for char particle conversion in environments containing O_2 and CO_2. *Combust. Flame* **2015**, *162*, 1455−1463.

(16) Haynes, B. S. A turnover model for carbon reactivity I. development. *Combust. Flame* **2001**, *126*, 1421−1432.

(17) *GRI-Mech 3.0*; http://combustion.berkeley.edu/gri_mech/overview.html (accessed Aug 2014).

(18) Haugen, N. E. L.; Mitchell, R. E. Modeling radiation in particle clouds: On the importance of inter-particle radiation for pulverized solid fuel combustion. *Heat Mass Transfer* **2015**, *51*, 991−999.

(19) Thiele, E. W. *Ind. Eng. Chem.* **1939**, *31*, 916.

(20) GASEQ. http://www.gaseq.co.uk/.

(21) *Cantera*; https://en.wikipedia.org/wiki/Cantera.

DOI: 10.1021/acs.energyfuels.6b00502
Energy Fuels XXXX, XXX, XXX−XXX